

# High Resolution Transmission Spectroscopy as a Diagnostic for Jovian Exoplanet Atmospheres: Constraints from Theoretical Models

Eliza M.-R. Kempton

Department of Physics, Grinnell College, Grinnell, IA 50112

kemptone@grinnell.edu

Rosalba Perna

Department of Physics and Astronomy, Stony Brook University, Stony Brook, NY, 11794

Kevin Heng

University of Bern, Center for Space and Habitability, Sidlerstrasse 5, CH-3012, Bern,  
Switzerland

Received \_\_\_\_\_; accepted \_\_\_\_\_

## ABSTRACT

We present high resolution transmission spectra of giant planet atmospheres from a coupled 3-D atmospheric dynamics and transmission spectrum model that includes Doppler shifts which arise from winds and planetary motion. We model jovian planets covering more than two orders of magnitude in incident flux, corresponding to planets with 0.9 to 55 day orbital periods around solar-type stars. The results of our 3-D dynamical models reveal certain aspects of high resolution transmission spectra that are not present in simple 1-D models. We find that the hottest planets experience strong substellar to anti-stellar (SSAS) winds, resulting in transmission spectra with net blue shifts of up to  $3 \text{ km s}^{-1}$ , whereas less irradiated planets show almost no net Doppler shifts. We find only minor differences between transmission spectra for atmospheres with temperature inversions and those without. Compared to 1-D models, peak line strengths are significantly reduced for the hottest atmospheres owing to Doppler broadening from a combination of rotation (which is faster for close-in planets under the assumption of tidal locking) and atmospheric winds. Finally, high resolution transmission spectra may be useful in studying the atmospheres of exoplanets with optically thick clouds since line cores for very strong transitions should remain optically thick to very high altitude. High resolution transmission spectra are an excellent observational test for the validity of 3-D atmospheric dynamics models, because they provide a direct probe of wind structures and heat circulation. Ground-based exoplanet spectroscopy is currently on the verge of being able to verify some of our modeling predictions, most notably the dependence of SSAS winds on insolation. We caution that interpretation of high resolution transmission spectra based on 1-D atmospheric models may be inadequate, as 3-D atmospheric motions can produce a noticeable effect on the absorption signatures.

*Subject headings:* planetary systems

## 1. Introduction

Transmission spectroscopy has been one of the most highly utilized methods in an astronomer’s repertoire for learning about exoplanet atmospheres. The absorption of stellar light through a planetary atmosphere leaves behind a spectral fingerprint of its chemical makeup, and can provide clues as to the many physical processes occurring in the atmosphere. To date, measurements of exoplanet transmission spectra have been accredited with the detection of molecules and atoms in exoplanet atmospheres (Burrows & Orton 2009, and references therein), along with providing evidence for disequilibrium chemistry, clouds or hazes (Pont et al. 2013; Deming et al. 2013; Sing et al. 2013; Kreidberg et al. 2014), winds, and orbital motion (Snellen et al. 2010). Typically, transmission spectra have been obtained at moderate to low spectral resolution in order to maximize the signal-to-noise ratio (SNR) of what is generally a very small signature relative to the bright background of the exoplanet host star. More recently, the first transmission spectra have been reported at much higher resolution ( $R \approx 10^5$ ) for the planet HD 209458b (Snellen et al. 2010). High resolution spectra have the advantage that individual spectral lines are fully resolved, as opposed to low resolution spectra where only broadband features can be probed. At high spectral resolution and high SNR, the line profiles of individual spectral lines can be used as valuable diagnostics of the physical processes taking place within an exoplanet atmosphere. This is comparable to methods used in stellar spectroscopy, where detailed information on abundance profiles, stellar structure, and even 3-D effects can be recovered from high SNR spectra. The obvious downside to high resolution transmission spectroscopy is that many more photons must be obtained in order to produce a high SNR spectrum. Because of this limitation, high resolution transmission spectroscopy has been limited so far to the very brightest host stars harboring transiting giant planets, and the spectra obtained still typically have quite low SNR. This situation is likely to improve as next generation of 30 to 40 meter class telescopes come online.

The geometry of the transit is such that the transmission spectrum probes a particularly interesting region of the exoplanet atmosphere. Absorption of stellar light occurs across the terminator – the region of the exoplanet atmosphere that lies between the substellar (day) side of the planet and the anti-stellar (night) side. This region of the atmosphere is problematic for modeling with 1-D atmospheric models, since the transport of both heat and atmospheric gas across the terminator can be significant. This is especially true for tidally-locked planets with a permanent fixed day-night boundary, where, depending on the nature of the day-night heat transport, the temperature difference between the two sides of the planet can be large (e.g. Showman et al. 2009; Dobbs-Dixon et al. 2010; Rauscher & Menou 2010; Heng et al. 2011b; Thrastarson & Cho 2011). In order to properly account for the atmospheric circulation that results, 3-D atmosphere models are required.

Previous modeling results calculating exoplanet transmission and emission at low spectral resolution with 3-D general circulation models (GCMs) often find good agreement with 1-D models. However, some inconsistencies have been shown to arise, especially in cases of strong chemical gradients or condensation of a key absorber between the day and night sides of the planet (Iro et al. 2005; Fortney et al. 2010; Burrows et al. 2010). These previous works have typically only considered the 3-D temperature structure of the atmosphere, while atmospheric motions have been ignored. At high spectral resolution however, 3-D atmospheric motions cannot be ignored, especially for cases where the magnitude of the motion exceeds the velocity resolution of the spectrograph in use. Observationally, this has been shown in a tantalizing manner by Snellen et al. (2010). These authors reported a  $2 \pm 1 \text{ km s}^{-1}$  blueshift in the high resolution transmission spectrum obtained for HD 209458b. While detected only at marginal significance, this result has been attributed to high altitude substellar to anti-stellar (SSAS) winds resulting from rapid flow from the hot day-side to the cooler night-side of the tidally locked planet. By generating transmission spectra from 3-D atmospheric circulation models including the Doppler shifts that arise from atmospheric

motions, both Miller-Ricci Kempton & Rauscher (2012) and Showman et al. (2013) find that day-to-night flow should produce a net blueshift of approximately  $2 \text{ km s}^{-1}$  in the transmission spectrum of HD 209458b – in agreement with the observational result.

The detection of Doppler shifts in exoplanet transmission spectra is powerful indeed. Miller-Ricci Kempton & Rauscher (2012) point out that high signal-to-noise observations could be used in the future to map out the wind structure on the approaching and receding limbs of a planet by measuring Doppler shifts in transmission spectra during ingress and egress. Spectral lines originating from different locations in the atmosphere could furthermore be used to map the wind structure as a function of altitude. This type of observation will likely require next generation 30 to 40 m class telescopes to realize but could ultimately provide a more complete picture of exoplanet meteorology. In the meantime, average Doppler shifts obtained over an entire portion of the transmission spectrum can provide a measure of the mean line-of-sight wind speed in an exoplanet atmosphere. Previous works by Perna et al. (2012) and Showman et al. (2013) predict that tidally locked hot Jupiters experiencing a high level of insolation should have strong day-side to night-side winds, whereas cooler planets on longer orbits will have less vigorous heat recirculation. These SSAS winds are most coherent in the upper atmosphere at pressures less than 10 mbar, which is precisely the location in the atmosphere where transmission spectra originate. The effects of the SSAS wind would therefore be apparent in the transmission spectrum via a net Doppler blue shift since the winds are directed towards the observer while the planet is transiting — exactly as seen in the Snellen et al. (2010) observations of HD 209458b.

Since the alleged detection of winds in the atmosphere of HD 209458b, several other hot Jupiter atmospheres have been observed at high spectral resolution using the CRILES instrument on the VLT (Kaeufl et al. 2004), which has a resolving power of up to  $10^5$ . The

hot Jupiters  $\tau$  Boötis b (Brogi et al. 2012; Rodler et al. 2012), HD 189733 b (de Kok et al. 2013; Birkby et al. 2013), and 51 Peg b (Brogi et al. 2013) have had their dayside *emission* spectra observed at high resolution, revealing molecular constituents of their atmospheres. Furthermore, at slightly lower resolution ( $R \approx 25,000$ ) a detection of water vapor was recently reported in the atmosphere of the non-transiting hot Jupiter  $\tau$  Boötis b from observations using the NIRSPEC instrument on the Keck telescopes (Lockwood et al. 2014). While CRIRES is currently the only instrument capable of measuring transmission spectra at  $R \geq 10^5$ , a variety of high resolution spectrographs are currently being planned for operation on the next generation of 30 to 40 m class telescopes. Of these, G-CLEF on the GMT (Szentgyorgyi et al. 2012), HROS on the TMT (Crampton et al. 2008), and the proposed CODEX (Pasquini et al. 2010), SIMPLE (Origlia et al. 2010), and HIRES (Maiolino et al. 2013) instruments for the E-ELT will have spectral resolution of approximately  $10^5$ , which should provide a powerful complement to the telescopes’ large mirror sizes. Spectra obtained with these instruments will open the door in the future to a wide array of exoplanet atmospheric diagnostics (e.g. Snellen 2013).

In this paper, we expand upon the previous work of Miller-Ricci Kempton & Rauscher (2012) and Showman et al. (2013) to study the effects of 3-D atmospheric structure and atmospheric circulation on high resolution exoplanet transmission spectra, including the Doppler shifts that arise from winds and the planet’s rotation. We extend the previous results to the study of planets ranging across more than two orders of magnitude in incident flux. We furthermore study the effects of stratospheric temperature inversions on the spectra. To accomplish this, we have coupled together the transmission spectrum model described in Miller-Ricci et al. (2009) and Miller-Ricci & Fortney (2010) with the atmospheric dynamics models of Perna et al. (2012) to produce transmission spectra that self-consistently treat the underlying 3-D atmospheric structure and circulation. The methodology is similar to that of Miller-Ricci Kempton & Rauscher (2012) and

Showman et al. (2013) but is applied across a broader range of parameter space to study tidally locked hot jovian planets as a population. We furthermore extend our study to hot Jupiters with layers of optically thick clouds, and we comment on how high resolution transmission spectra can be used to constrain the properties of these atmospheres. Our modeling methods are laid out in Section 2. Results are presented in Section 3 and we finish with concluding remarks in Section 4.

## 2. Model Description

### 2.1. 3-D Dynamics Models

For our study, we use the same suite of 16 atmospheric circulation models computed by Perna et al. (2012, PHP in the following), using the numerical setup described in (Heng et al. 2011a,b). A detailed description of the models, as well as the numerical techniques employed, can be found in the above papers, and hence in the following we will limit ourselves to summarize the main features and describe the updates that have been made since the publication of PHP<sup>1</sup>.

The 16 models are computed for 8 values of the irradiation temperature  $T_{\text{irr}}$  in the range  $\approx 770 - 3000$  K. The effective stellar temperature  $T_*$  and stellar radius  $R_*$  are related to the irradiation temperature by the relation

$$T_{\text{irr}} = T_* \left( \frac{R_*}{a} \right)^{1/2}, \quad (1)$$

where  $a$  is the semi-major axis of the orbiting exoplanet. Given an irradiating flux

---

<sup>1</sup> We remind that those models do not include magnetic drag, which is known to reduce wind speeds if the atmosphere is strongly magnetized (Perna et al. 2010; Rogers & Showman 2014).



$\mathcal{F}_0 = \sigma_{\text{SB}} T_{\text{irr}}^4$ , this is expressed by

$$a = R_{\star} T_{\star}^2 \left( \frac{\sigma_{\text{SB}}}{\mathcal{F}_0} \right)^{1/2} \approx 0.09 \text{ AU} \left( \frac{R_{\star}}{R_{\odot}} \right) \left( \frac{T_{\star}}{6000 \text{ K}} \right)^2 \left( \frac{\mathcal{F}_0}{2 \times 10^8 \text{ erg cm}^{-2} \text{ s}^{-1}} \right)^{-1/2}, \quad (2)$$

where  $\sigma_{\text{SB}}$  is the Stefan-Boltzmann constant and the mass  $M_{\star}$  of the host star is taken to be one solar mass. The planet is assumed to be tidally locked, which is generally a good approximation for the models considered here (see PHP for details). The orbital frequency (equal to the rotational one), is then given by  $\Omega_p \approx (GM_{\star}/a^3)^{1/2}$ . With this setup, for each irradiation temperature  $T_{\text{irr}}$ , the values for  $\mathcal{F}_0$ ,  $\Omega_p$  and  $a$  are correspondingly determined according to the relations above. The numerical values of these quantities are reported in Table 1.

For each of the 8 values of the irradiation temperature in Table 1, we consider a circulation model with temperature inversion, and another without. In the absence of clouds and hazes, the use of the dual-band approximation for radiative transfer (e.g. Heng et al. 2011b) allows for establishing the presence of a temperature inversion by means of the magnitude of the ratio  $\gamma_0 \equiv \kappa_{\text{S}}/\kappa_0$ , where  $\kappa_{\text{S}}$  is the shortwave (optical) opacity, and  $\kappa_0$  is the longwave opacity. If  $\gamma_0 > 1$ , the shortwave photosphere sits above the longwave photosphere and an inversion exists; if  $\gamma_0 < 1$ , the relative locations of the two photospheres are reversed, and there is no inversion. For the former situation, we consider a case with  $\gamma_0 = 2$ , while for the latter we take  $\gamma_0 = 0.5$ . As described in PHP, the simulations make the simple assumption that temperature inversions (or their absence) may be maintained over the entire atmosphere, as a means of isolating their effects on the results, commensurate with the fact that the identity of these "stratospheric absorbers" remains basically unknown.

Global-mean temperature-pressure profiles for all 16 models are shown in Fig. 1, with the pressure range relevant for absorption studies (approximately 0.1 - 10 mbar)

indicated. Since the publication of PHP, the upper boundary of the models has been extended to 10  $\mu$ bar to include the portion of the atmosphere probed by transmission spectroscopy. The equilibrium condition for CO and CH<sub>4</sub> to be present in equal quantities is indicated in Figure 1 as well. For all of our models except the coldest ones (C, C1, and C2) CO is expected to be the dominant carbon-bearing molecule in the region of the atmosphere probed by transmission spectroscopy. It should be noted however that 3-D effects can produce more (or less) CO in hotter (or colder) regions of the atmosphere, and non-equilibrium chemistry may further alter the abundances of carbon-bearing molecules beyond their calculated values (Cooper & Showman 2006). The former effect is accounted for in our modeling. The latter is not, as we only compute abundances in thermochemical equilibrium (see Miller-Ricci et al. 2009)

## 2.2. Transmission Spectroscopy Model

We have coupled the transmission spectroscopy model described in Miller-Ricci et al. (2009) and Miller-Ricci & Fortney (2010), with the 3-D atmospheric circulation models from PHP. The coupling of the two models is essentially the same as the one described in Miller-Ricci Kempton & Rauscher (2012). Briefly, light rays are passed through the upper atmosphere of the planet, accounting for the geometry of the grazing trajectory for stellar light through the planetary atmosphere during transit. The attenuation of stellar light is calculated by integrating the transfer equation for the case of absorption only, along the path of the light

$$I(\lambda) = I_0 e^{-\tau}, \quad (3)$$

where  $I_0$  is the incident intensity from the star. The total absorption is then found by integrating the individual light rays over the entire annulus of the planetary atmosphere, as viewed by an observer on Earth.

At each location in the atmosphere — defined by its latitude, longitude, and height coordinates — the opacity,  $\kappa$  (in units of  $\text{cm}^2 \text{ g}^{-1}$ ), is determined for solar composition gas in chemical equilibrium at the local temperature and pressure. The optical depth  $\tau$  from Equation 3 is then obtained according to

$$\tau = \int \rho \kappa ds, \quad (4)$$

where  $ds$  is the differential path length computed along the observer’s line of sight, and  $\rho$  is the gas density. In order to account for atmospheric motions resulting from winds and the planet’s rotation, we Doppler-shift the opacity at each location in the atmosphere according to the local line-of-sight (LOS) velocity. At the center of transit time, the LOS velocity is given by

$$v_{LOS} = -[u \sin \theta \cos \phi + v \cos \theta \sin \phi + (R_p + z)\Omega_p \sin \theta \cos \phi] \quad (5)$$

where  $u$  and  $v$  are the zonal and meridional components of the windspeed respectively,  $\phi$  and  $\theta$  are the latitude and longitude,  $R_p$  is the planetary radius, and  $z$  is the altitude above the 1-bar pressure location. We neglect the vertical component of the windspeed, since it does not contribute significantly to  $v_{LOS}$  at the terminator due to geometric effects. Furthermore, the vertical winds are typically at least two orders of magnitude smaller than the zonal ones. By incorporating the Doppler-shifted opacities into our 3-D calculation, we produce transmission spectra that are consistent with the underlying 3-D atmospheric structure and wind pattern.

### 3. Results

#### 3.1. Temperature-Dependent Effects

Spectra for each of the 16 models are shown in Figure 2 for a calculation without the Doppler shifting effects of winds or planetary rotation included. The spectra appear

qualitatively similar for the models with and without temperature inversions. The strong resemblance between models with very different temperature structure is unsurprising. Transmission spectra arise from pure absorption through the atmosphere, which has only a minor dependence on temperature, insofar as the gas opacities (and associated chemistry) vary slowly as a function of  $T$ . For the same reason we also find that the spectra calculated without any Doppler shifts applied are qualitatively similar to spectra calculated using a 1-D T-P profile that is the average of all of the profiles from the 3-D model (not shown), in agreement with prior work by Fortney et al. (2010). Going from hottest to coldest, the most obvious change in the unshifted spectra is the decrease in line strength that results from the reduction in atmospheric scale height, which is in turn proportional to temperature. Also, for the very coldest models, more carbon is incorporated into  $\text{CH}_4$  than  $\text{CO}$ , resulting in a complex forest of  $\text{CH}_4$  lines appearing in the spectra for these models. The transition from  $\text{CO}$  to  $\text{CH}_4$  takes place at lower  $T_{irr}$  for the models with temperature inversions than for those without. Even for the very coldest model (C), some  $\text{CO}$  absorption still remains in the transmission spectrum for the model with  $\gamma = 2.0$ . At all levels of planetary irradiation, the  $\text{CO}$  absorption is slightly stronger in the temperature inversion models, owing to the higher temperature at altitude, which produces a correspondingly larger scale height along with slightly higher  $\text{CO}$  abundance in the region where the transmission spectrum originates. This is a very small effect however, and the unshifted spectra imply that it will remain very difficult to distinguish between models with differing temperature structure using transmission spectra observations.

When the Doppler shifts resulting from winds and planetary rotation are self-consistently included in the modeling of the transmission spectra, peak line strengths are considerably reduced and individual spectral lines are correspondingly broadened (see Figure 3). The spectra for the hottest planets are substantially blue shifted, which we discuss in detail in the following subsection. For tidally locked planets, the hottest models

experience the most significant rotational broadening. This results from the short orbital periods and correspondingly short rotation periods for the hottest planets. As a result, the larger scale height of the hot atmospheres, which would typically produce much stronger absorption features, is mitigated to a large extent by a reduction in line strength from more extreme rotational broadening. The advantage of observing hot planets in transmission is therefore substantially reduced. For high resolution spectra under conditions where the spectral resolution  $R > c/v_{rot}$ , it should be noted that 1-D models that do not at least include effects of rotational broadening might over-predict the strength of spectral lines in transmission spectra by a factor of several.

### 3.2. Atmospheric Winds

In addition to the rotational broadening, atmospheric circulation for the hottest jovian planets has an appreciable effect on the transmission spectra. Whereas rotational broadening has an (almost) symmetrical effect on spectral lines, winds can produce highly asymmetric perturbations to spectral lines profiles (e.g. Miller-Ricci Kempton & Rauscher 2012; Showman et al. 2013). The effects of winds can only be modeled through 3-D calculations such as the ones presented here. 1-D models entirely miss out on the significant effects of winds on transmission spectra, which become apparent at high resolution, as seen in Figure 3. The transmission spectrum originates from high in the atmosphere ( $P_{atm} \sim 1$  mbar), where the atmospheric circulation is predominantly advective, resulting in direct transport of hot dayside gas across the terminator to the colder night side of the planet. The transit geometry guarantees that the day-to-night winds will be directed toward the observer along his/her sightline, producing a net blue shift in the absorption signature of the exoplanet atmosphere.

The blue shifting of hot Jupiter transmission spectra is apparent from our models in

Figure 3, where a slight shift to shorter wavelengths can be seen by eye in the spectra of the hottest planets. Wind speeds are typically larger for the hotter exoplanets, and the high altitude day-to-night flow is more coherent, resulting in larger net blueshifts for the more highly irradiated atmospheres. The strong SSAS flow for the hottest models can be explained in the following way, as pointed out originally by Showman & Guillot (2002). In highly irradiated gas giants, the flow is expected to occur roughly at the sound speed. This means that the dynamical timescale can be given by  $t_{dyn} \sim R_p/c_s$ . It follows that

$$\frac{t_{rad}}{t_{dyn}} \sim \frac{c_P P c_s}{g \sigma_{SB} T^3 R_p} \propto \frac{P}{T^{5/2}}. \quad (6)$$

The gas heat capacity, surface gravity, and planetary radius ( $c_P$ ,  $g$ , and  $R_p$ ) are held constant in our simulations, and the relevant pressure is taken to be the photospheric pressure. Atmospheres with higher values of  $t_{rad}/t_{dyn}$  are therefore colder and have flows that are more zonal in nature with comparable red- and blue shifted components. Those with lower values of the ratio are hotter and have more prevalent SSAS flow.

The LOS components of the exoplanet winds around the terminator are shown in Figure 4. The behavior is essentially as described above. The winds become significantly weaker for models with lower  $T_{irr}$ . Additionally, the suite of models with the exception of the coldest one (model C) displays a slow transition from SSAS flow to more zonal flow as the irradiating flux is diminished. In the case of model C, the flow transitions abruptly back to being strongly SSAS, which likely results from differences in opacities. Model C is the only one in the suite where carbon is almost exclusively bound up in  $\text{CH}_4$ , rather than  $\text{CO}$ , which affects the radiative transfer.

At this point in time, observers are typically not able to obtain high resolution transmission spectra at high signal-to-noise, like the ones shown in Figures 2 and 3. Instead, information about the transmission spectrum is recovered by cross correlating the entire observed spectrum against a template. The template is typically chosen to be a modeled

spectrum of the system in question. The best fit parameters of the planetary atmosphere are then inferred by locating the highest significance peak in the cross correlation function. For consistency with the observational method, we have cross-correlated our Doppler-shifted transmission spectrum models against their unshifted counterparts (shown in Figure 2), which serve as template spectra. The net Doppler shift obtained from the cross correlation process gives a measure of the average LOS velocity in the upper atmosphere of the planet that would be recovered observationally.

Our results from the cross correlation process can be seen in Figure 5. We find large net blue shifts of 2 - 3 km s<sup>-1</sup> for the hottest exoplanets, and there is a gradual shift to no discernible blue-shift for the least irradiated of our models. Planets both with and without temperature inversions show the same qualitative behavior. However, at most levels of irradiation, the models with temperature inversions produce larger net blue shifts by up to about 1 km s<sup>-1</sup>. This follows again from Equation 6 — the transmission spectrum probes hotter regions of the atmospheres with inversions, which are more radiative, thus producing stronger SSAS flow. As a result, the gradual transition from large blue shift to no blue shift begins at a lower irradiation level for the T-inversion models than for those without inversions. For the  $\gamma = 2.0$  models, we predict that HD 209458b and HD 189733b should both have large net Doppler blue shifts in their transmission spectra of  $\approx 3$  km s<sup>-1</sup>, whereas the  $\gamma = 0.5$  models predict a weaker blue shift for HD 189733b than for HD 209458b. These conclusions are in line with the work of Showman et al. (2013) who predicted a smaller net blue shift for the less irradiated HD 189733b, although with a larger rotational broadening component due to HD 189733b traversing a tighter orbit around a cooler star than HD 209458. Observational confirmation of the net blue shifts for the transmission spectra of these two planets in particular, along with other giant planets orbiting bright stars, may be possible in the coming years, as evidenced by the work on HD 209458b by Snellen et al. (2010), which would provide useful validation of our modeling results.

### 3.3. Clouds

Recently, convincing evidence has been presented that clouds and/or hazes play a considerable role in the transmission spectra of a wide variety of exoplanet atmospheres (e.g. Kreidberg et al. 2014; Sing et al. 2013; Pont et al. 2013). The nature of the cloud particles is unknown at this time, but they appear to be a prevalent feature in irradiated exoplanet atmospheres, and many radiative transfer models are poorly equipped to deal with their presence. From the observational standpoint, clouds are a hindrance to inferring the composition of an exoplanet atmosphere via transmission spectroscopy. Layers of high altitude clouds or hazes can create an optically thick barrier, preventing observation of deeper layers of the atmosphere where atomic and molecular spectral features would otherwise originate. In low spectral resolution observations, this effect can also be misconstrued with the reduced scale height associated with high metallicity. The flattening or smoothing of the transmission spectrum as a result of clouds is a well-documented phenomenon that can confound efforts to measure the composition of an exoplanet’s atmosphere. This has been particularly problematic in the case of the super-Earth GJ 1214b. Measurements of the bulk density of the planet imply that it must have a substantial gaseous atmosphere (Rogers & Seager 2009; Nettelmann et al. 2011; Valencia et al. 2013). However, observations of the planet’s transmission spectrum at ever increasing precision continue to reveal a flat spectrum, which is now only consistent with the presence of a high thick layer of clouds (Kreidberg et al. 2014). To resolve the problem of what such an atmosphere is composed of, high resolution spectroscopy may be the answer. While at low resolution, the transmission spectrum might appear entirely flat, narrow strong spectral lines should still remain optically thick above the cloud deck. At high spectral resolution, these lines could therefore be observed, and an atmospheric composition inferred from their presence.



We have performed limited tests of the effects of high altitude clouds on hot Jupiter transmission spectra by truncating absorption of stellar light at the height of an arbitrarily inserted cloud deck. Clouds are inserted at 100, 10, 1,  $10^{-1}$  mbar, and  $10^{-2}$  mbar, and the results for one of our model atmospheres (model H) are shown in Figure 6. The signal drops precipitously as the height of the cloud deck is increased, however some signal remains present up to cloud decks at 0.1 mbar. While it will likely prove challenging observationally to detect molecular signatures from above a high cloud deck, high resolution transmission spectroscopy of narrow, but strong, spectral features may provide the only tenable path forward in this regard.

#### 4. Conclusions

Our grid of jovian planet atmosphere models reveals that transmission spectra at high resolution can be used to probe a variety of atmospheric physics. We have found that even at very high spectral resolution, transmission spectra are not strongly dependent on the temperature structure for an atmosphere. While it is unfortunate that transmission spectra do not reveal much information about atmospheric temperature structure, this removes a significant source of degeneracy that is typically present in the interpretation of emission spectra. As a result, transmission spectra can be used as a relatively unambiguous probe for atmospheric composition and wind structure, without the worry of convoluting these effects with other temperature-dependent effects. While we find some minor differences between transmission spectra for atmospheres with temperature inversions relative to those without, these differences are likely too small to be observable in the near future.

The effects of winds on jovian planet transmission spectra however, can be substantial. Significant rotational broadening is expected for hot Jupiters on close-in orbits, and day-to-night winds will imprint a net blueshift on the transmission spectra of up to several

km s<sup>-1</sup>. The finding that the most strongly irradiated jovian planets should produce transmission spectra with the largest net Doppler blue shifts provides a testable hypothesis from our results. Previous studies that claim close resemblance between 1-D and 3-D modeled transmission spectra (Fortney et al. 2010) remain valid at low spectral resolution, but we have shown here that 3-D models depart significantly from their 1-D counterparts when dynamical effects are taken into account, especially for the hottest exoplanets.

Our work in this paper extends the previous studies of Showman et al. (2013) who looked at three specific exoplanets – HD 209458b, HD 189733b, and GJ 436b – to see how stellar insolation affects the atmospheric dynamics and alters the resulting Doppler shifted transmission spectra. The authors reported a "regime shift" between strong SSAS flow for the heavily irradiated HD 209458b and zonal flow for the colder planet GJ 436b. In our current work, rather than modeling three individual planets with different radii, surface gravities, and stellar hosts, we provide a well-defined (and well-sampled) grid of models to more carefully study the effects of insolation on Doppler shifted transmission spectra. In our suite of models we observe a similar shift in upper atmosphere dynamics from SSAS flow for hot planets to zonal flow colder planets. However, our shift is not as pronounced as what was reported in Showman et al. (2013), and we would hesitate to call it a regime shift. In fact, the development of jets and a zonal wind pattern appears to reverse itself in our very coldest models. Our coldest model (model C) has a strongly SSAS flow (see Figure 4), which likely results from changes in atmospheric carbon chemistry, which in turn affects opacities and the resulting radiative transfer at low levels of insolation. Like Showman et al. (2013) we do however, continue to see a reduction in the net Doppler blueshift as the level of insolation is reduced. This trend continues, all the way to the very coldest models. Our model C produces the smallest net blueshift overall, despite having strong SSAS flow in the upper atmosphere. The reason for this is straightforward – the average wind speeds fall off sharply with decreasing  $T_{irr}$ . Despite having coherent SSAS flow in model C, the

average wind speeds are so small that there is very little discernible blue shift in this model. As a result, we conclude that Doppler shifted transmission spectra will only be useful in determining the extent of SSAS vs. zonal flow for the most highly irradiated jovian planets. Cooler giant planets will have slower wind speeds overall, and it therefore becomes much more challenging to use Doppler-shifted transmission spectra to diagnose the planet-wide wind structure – even when observations are obtained with very high spectral resolution.

As for why we do not observe a strong regime shift in our models as a function of insolation, the differences between our suite of models and those of Showman et al. (2013) are difficult to fully diagnose without performing a true one-to-one comparison. However, we can offer up a couple of suggestions. First of all, the treatment of atmospheric drag is not identical between our two suites of models. It has previously been shown in both Miller-Ricci Kempton & Rauscher (2012) and Showman et al. (2013) that the treatment of atmospheric drag can have substantial effects on atmospheric circulation, which in turn alters the degree of blue-shifting of the transmission spectra. In our suite of models we do not provide any prescription for drag from magnetic fields or shocks, but our simulations do explicitly include numerical dissipation to stabilize against numerical noise such that they are able to run to completion. Generally, simulations of atmospheric circulation inevitably include some form of numerical dissipation, even if not explicitly applied, via the computational grid and numerical scheme. Our choice, as laid out in PHP, has been to apply a single planet-wide numerical dissipation factor that is proportional to  $1/\Omega$ , where  $\Omega$  is the rotational frequency. Heng et al. (2011b) point out that wind speeds from 3-D GCMs are uncertain at the  $\sim 10\%$  level, depending on how one specifies the numerical dissipation / drag. This is likely to be the key source for the differences in circulation patterns between our own models and those of Showman et al. (2013). Another potential difference comes from the rotation rates of our models. All three planets modeled in Showman et al. (2013) have similar orbital (and therefore rotational) periods of close to 3 days, whereas our coldest

modeled planets have rotation periods of approximately 56 days. These differences in rotation rate may bring about subtle changes to the atmospheric dynamics. Showman et al. (2009), Kataria et al. (2013), and Rauscher & Kempton (2014) have studied the effects of rotation rate on atmospheric dynamics for non-tidally locked planets and/or planets on eccentric orbits, and all of these authors report substantial changes in atmospheric circulation by altering the planetary rotation rate. However, it is not clear how relevant these previous results are to our current conclusions, as the dynamical effects produced in the three aforementioned papers probably result in large part from the very different stellar forcing brought about by the non-tidally locked and eccentric orbital configuration of their models.

The use of cross correlation techniques to recover information from high resolution transmission spectra results in the entire spectrum being used simultaneously for interpretation, rather than direct observations of individual spectral features. These techniques typically rely upon a model spectrum as a template for the spectral recovery process, and the template spectra have typically have been produced from 1-D radiative transfer models. The assumption is that the template is an accurate representation of the observed spectrum. If this is not the case, inconsistencies may arise in the interpretation of the data. This necessitates asking the question of whether these cross correlation techniques have unexplored degeneracies, which might limit the accuracy at which planetary properties can be discerned. de Kok et al. (2014) have studied the conditions under which atmospheric composition and other planetary properties can be recovered from high resolution transmission spectra via cross correlation techniques. However, the authors limited their study to 1-D models (and  $1D \times 2$  models where separate 1-D profiles were used for the day side and the night side of the planet). As we have demonstrated here, 3-D effects become discernible at high spectral resolution, and it would therefore be unwise to ignore these effects until their impact on spectral recovery methods have been fully studied.

In certain cases — especially for the most highly irradiated planets in our study, as well as those on the  $\text{CH}_4$  /  $\text{CO}$  equilibrium boundary — our models reveal a large enough discrepancy between 1-D and 3-D models that the 3-D effects might alter the interpretation of the spectra.

In the era of 30 to 40 m class telescopes, high resolution spectroscopy of exoplanet atmospheres will be a valuable tool for exoplanet characterization. As we have shown, winds in exoplanet atmospheres can be diagnosed by high resolution spectroscopy, so long as the resolution of the spectrograph is at least of order  $v/c$ , where  $v$  is the typical LOS wind speed. For winds  $\sim 1 \text{ km s}^{-1}$ , this requires spectroscopy at a resolution of at least  $10^5$ . In addition to spectroscopy of hot jupiters, it may be possible to characterize habitable terrestrial planets (Snellen et al. 2013; Rodler & López-Morales 2014) and even to extract planetary masses directly from transmission spectra (de Wit & Seager 2013). The use of ground-based facilities with high resolution spectrographs, in conjunction with space-based observations that are typically limited to much lower spectral resolution, will therefore allow for detailed studies of exoplanet atmospheres that are not accessible at present. This includes observations of Doppler shifted transmission spectra, which will provide valuable constraints on the nature of the atmospheric circulation in exoplanet atmospheres.

KH acknowledges support from the Swiss National Science Foundation and the Swiss-based MERAC Foundation.

## REFERENCES

- Birkby, J. L., de Kok, R. J., Brogi, M., de Mooij, E. J. W., Schwarz, H., Albrecht, S., & Snellen, I. A. G. 2013, MNRAS, 436, L35
- Brogi, M., Snellen, I. A. G., de Kok, R. J., Albrecht, S., Birkby, J., & de Mooij, E. J. W. 2012, Nature, 486, 502
- Brogi, M., Snellen, I. A. G., de Kok, R. J., Albrecht, S., Birkby, J. L., & de Mooij, E. J. W. 2013, ApJ, 767, 27
- Burrows, A. & Orton, G. 2009, ArXiv e-prints
- Burrows, A., Rauscher, E., Spiegel, D. S., & Menou, K. 2010, ApJ, 719, 341
- Cooper, C. S. & Showman, A. P. 2006, ApJ, 649, 1048
- Crampton, D., Simard, L., & Silva, D. 2008, in Society of Photo-Optical Instrumentation Engineers (SPIE) Conference Series, Vol. 7014, Society of Photo-Optical Instrumentation Engineers (SPIE) Conference Series
- de Kok, R. J., Birkby, J., Brogi, M., Schwarz, H., Albrecht, S., de Mooij, E. J. W., & Snellen, I. A. G. 2014, A&A, 561, A150
- de Kok, R. J., Brogi, M., Snellen, I. A. G., Birkby, J., Albrecht, S., & de Mooij, E. J. W. 2013, A&A, 554, A82
- de Wit, J. & Seager, S. 2013, Science, 342, 1473
- Deming, D., Wilkins, A., McCullough, P., Burrows, A., Fortney, J. J., Agol, E., Dobbs-Dixon, I., Madhusudhan, N., Crouzet, N., Desert, J.-M., Gilliland, R. L., Haynes, K., Knutson, H. A., Line, M., Magic, Z., Mandell, A. M., Ranjan, S., Charbonneau, D., Clampin, M., Seager, S., & Showman, A. P. 2013, ApJ, 774, 95

- Dobbs-Dixon, I., Cumming, A., & Lin, D. N. C. 2010, *ApJ*, 710, 1395
- Fortney, J. J., Shabram, M., Showman, A. P., Lian, Y., Freedman, R. S., Marley, M. S., & Lewis, N. K. 2010, *ApJ*, 709, 1396
- Heng, K., Frierson, D. M. W., & Phillipps, P. J. 2011a, *MNRAS*, 418, 2669
- Heng, K., Menou, K., & Phillipps, P. J. 2011b, *MNRAS*, 413, 2380
- Iro, N., Bézard, B., & Guillot, T. 2005, *A&A*, 436, 719
- Kaeuffl, H.-U., Ballester, P., Biereichel, P., Delabre, B., Donaldson, R., Dorn, R., Fedrigo, E., Finger, G., Fischer, G., Franza, F., Gojak, D., Huster, G., Jung, Y., Lizon, J.-L., Mehrgan, L., Meyer, M., Moorwood, A., Pirard, J.-F., Paufigue, J., Pozna, E., Siebenmorgen, R., Silber, A., Stegmeier, J., & Wegerer, S. 2004, in *Society of Photo-Optical Instrumentation Engineers (SPIE) Conference Series*, Vol. 5492, Society of Photo-Optical Instrumentation Engineers (SPIE) Conference Series, ed. A. F. M. Moorwood & M. Iye, 1218–1227
- Kataria, T., Showman, A. P., Lewis, N. K., Fortney, J. J., Marley, M. S., & Freedman, R. S. 2013, *ApJ*, 767, 76
- Kreidberg, L., Bean, J. L., Désert, J.-M., Benneke, B., Deming, D., Stevenson, K. B., Seager, S., Berta-Thompson, Z., Seifahrt, A., & Homeier, D. 2014, *Nature*, 505, 69
- Lockwood, A. C., Johnson, J. A., Bender, C. F., Carr, J. S., Barman, T., Richert, A. J. W., & Blake, G. A. 2014, *ApJ*, 783, L29
- Maiolino, R., Haehnelt, M., Murphy, M. T., Queloz, D., Origlia, L., Alcalá, J., Alibert, Y., Amado, P. J., Allende Prieto, C., Ammler-von Eiff, M., Asplund, M., Barstow, M., Becker, G., Bonfils, X., Bouchy, F., Bragaglia, A., Burleigh, M. R., Chiavassa, A., Cimatti, D. A., Cirasuolo, M., Cristiani, S., D’Odorico, V., Dravins, D., Emsellem,

- E., Farihi, J., Figueira, P., Fynbo, J., Gansicke, B. T., Gillon, M., Gustafsson, B., Hill, V., Israelyan, G., Korn, A., Larsen, S., De Laverny, P., Liske, J., Lovis, C., Marconi, A., Martins, C., Molaro, P., Nisini, B., Oliva, E., Petitjean, P., Pettini, M., Recio Blanco, A., Rebolo, R., Reiners, A., Rodriguez-Lopez, C., Ryde, N., Santos, N. C., Savaglio, S., Snellen, I., Strassmeier, K., Tanvir, N., Testi, L., Tolstoy, E., Triaud, A., Vanzi, L., Viel, M., & Volonteri, M. 2013, ArXiv e-prints
- Miller-Ricci, E. & Fortney, J. J. 2010, ApJ, 716, L74
- Miller-Ricci, E., Seager, S., & Sasselov, D. 2009, ApJ, 690, 1056
- Miller-Ricci Kempton, E. & Rauscher, E. 2012, ApJ, 751, 117
- Nettelmann, N., Fortney, J. J., Kramm, U., & Redmer, R. 2011, ApJ, 733, 2
- Origlia, L., Oliva, E., Maiolino, R., Gustafsson, B., Piskunov, N., Kochucov, O., Vanzi, L., Minniti, D., Zoccali, M., Hatzes, A., & Guenther, E. 2010, in Society of Photo-Optical Instrumentation Engineers (SPIE) Conference Series, Vol. 7735, Society of Photo-Optical Instrumentation Engineers (SPIE) Conference Series
- Pasquini, L., Cristiani, S., García López, R., Haehnelt, M., Mayor, M., Liske, J., Manescau, A., Avila, G., Dekker, H., Iwert, O., Delabre, B., Lo Curto, G., D’Odorico, V., Molaro, P., Viel, M., Vanzella, E., Bonifacio, P., di Marcantonio, P., Santin, P., Comari, M., Cirami, R., Coretti, I., Zerbi, F. M., Spanò, P., Riva, M., Rebolo, R., Israelian, G., Herrero, A., Zapatero Osorio, M. R., Tenegi, F., Carswell, B., Becker, G., Udry, S., Pepe, F., Lovis, C., Naef, D., Dessauges, M., & Mégevand, D. 2010, in Society of Photo-Optical Instrumentation Engineers (SPIE) Conference Series, Vol. 7735, Society of Photo-Optical Instrumentation Engineers (SPIE) Conference Series
- Perna, R., Heng, K., & Pont, F. 2012, ApJ, 751, 59



- Perna, R., Menou, K., & Rauscher, E. 2010, *ApJ*, 719, 1421
- Pont, F., Sing, D. K., Gibson, N. P., Aigrain, S., Henry, G., & Husnoo, N. 2013, *MNRAS*, 432, 2917
- Rauscher, E. & Kempton, E. M. R. 2014, *ApJ*, 790, 79
- Rauscher, E. & Menou, K. 2010, *ApJ*, 714, 1334
- Rodler, F. & López-Morales, M. 2014, *ApJ*, 781, 54
- Rodler, F., Lopez-Morales, M., & Ribas, I. 2012, *ApJ*, 753, L25
- Rogers, L. A. & Seager, S. 2009, *ArXiv e-prints*
- Rogers, T. M. & Showman, A. P. 2014, *ApJ*, 782, L4
- Showman, A. P., Fortney, J. J., Lewis, N. K., & Shabram, M. 2013, *ApJ*, 762, 24
- Showman, A. P., Fortney, J. J., Lian, Y., Marley, M. S., Freedman, R. S., Knutson, H. A., & Charbonneau, D. 2009, *ApJ*, 699, 564
- Showman, A. P. & Guillot, T. 2002, *A&A*, 385, 166
- Sing, D. K., Lecavelier des Etangs, A., Fortney, J. J., Burrows, A. S., Pont, F., Wakeford, H. R., Ballester, G. E., Nikolov, N., Henry, G. W., Aigrain, S., Deming, D., Evans, T. M., Gibson, N. P., Huitson, C. M., Knutson, H., Showman, A. P., Vidal-Madjar, A., Wilson, P. A., Williamson, M. H., & Zahnle, K. 2013, *MNRAS*, 436, 2956
- Snellen, I. 2013, in *European Physical Journal Web of Conferences*, Vol. 47, European Physical Journal Web of Conferences, 11001
- Snellen, I. A. G., de Kok, R. J., de Mooij, E. J. W., & Albrecht, S. 2010, *Nature*, 465, 1049
- Snellen, I. A. G., de Kok, R. J., le Poole, R., Brogi, M., & Birkby, J. 2013, *ApJ*, 764, 182

- Szentgyorgyi, A., Frebel, A., Furesz, G., Hertz, E., Norton, T., Bean, J., Bergner, H., Crane, J., Evans, J., Evans, I., Gauron, T., Jordán, A., Park, S., Uomoto, A., Barnes, S., Davis, W., Eisenhower, M., Epps, H., Guzman, D., McCracken, K., Ordway, M., Plummer, D., Podgorski, W., & Weaver, D. 2012, in Society of Photo-Optical Instrumentation Engineers (SPIE) Conference Series, Vol. 8446, Society of Photo-Optical Instrumentation Engineers (SPIE) Conference Series
- Thrastarson, H. T. & Cho, J. Y. 2011, ApJ, 729, 117
- Valencia, D., Guillot, T., Parmentier, V., & Freedman, R. S. 2013, ApJ, 775, 10

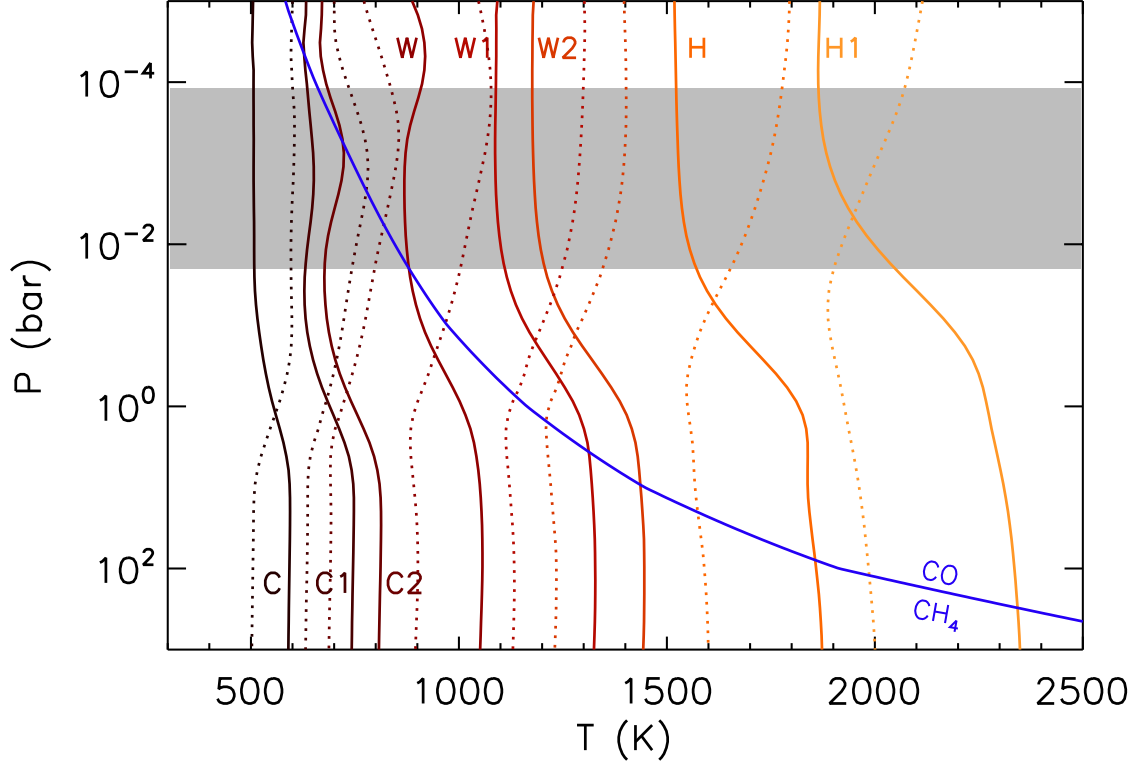


Fig. 1.— Global mean T-P profiles for the models presented in this paper. The profiles shown were computed by taking a planet-wide average of the individual T-P profiles from our model grid of 96 latitude by 192 longitude grid points. The gray shaded region indicates the portion of the atmosphere typically probed by transmission spectroscopy. The CO / CH<sub>4</sub> equilibrium line is indicated in blue.

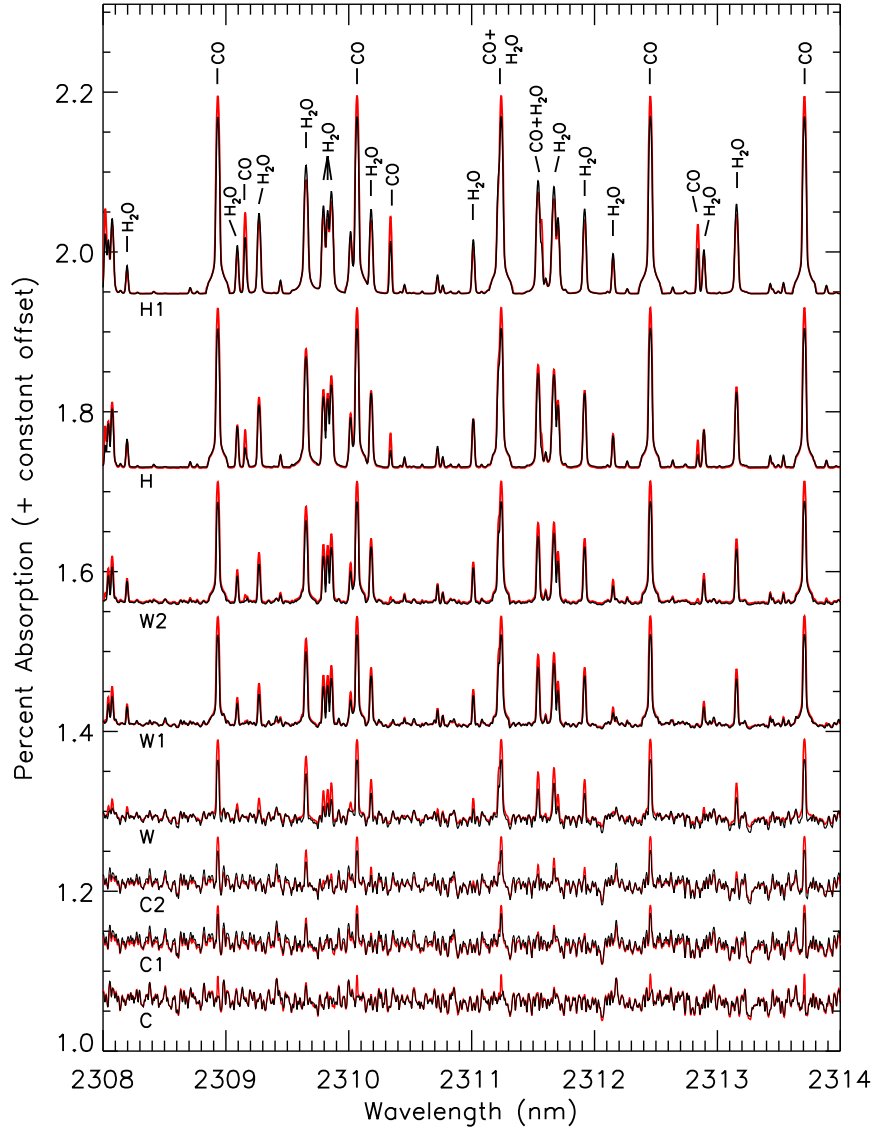


Fig. 2.— Transmission spectra for the 16 model atmospheres considered in this paper. No Doppler shifting of spectral lines has been applied to these spectra. Models go from hottest at the top, to coldest at the bottom. Red lines are for atmospheres with T-inversions. Black lines are atmospheres with no inversions. An arbitrary vertical offset has been added to each spectrum for easier viewing. CO and H<sub>2</sub>O absorption features are indicated. (The vast majority of the unmarked features in the spectra of the colder planets are due to methane. The flat “continuum” opacity source in the hottest models results from collision-induced absorption of H<sub>2</sub>-H<sub>2</sub> and H<sub>2</sub>-He pairs.)

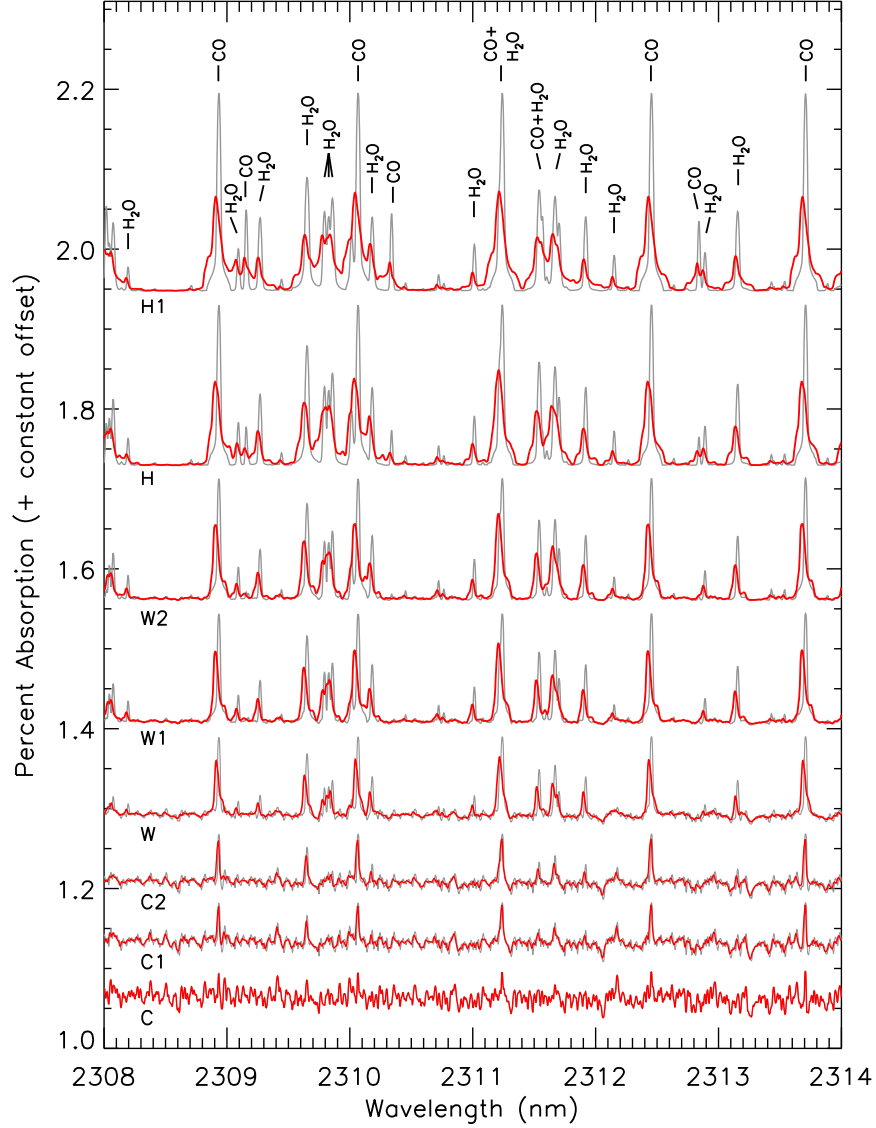


Fig. 3.— Doppler shifted transmission spectra for the 8 models with temperature inversions ( $\gamma = 2.0$ , red lines). Gray lines are the unshifted spectra from Figure 2, shown for reference. An analogous figure for the non-inverted models ( $\gamma = 0.5$ ) is not shown but looks qualitatively the same. Rotational broadening and a net blueshift due to day-to-night winds is most apparent for the hottest models.

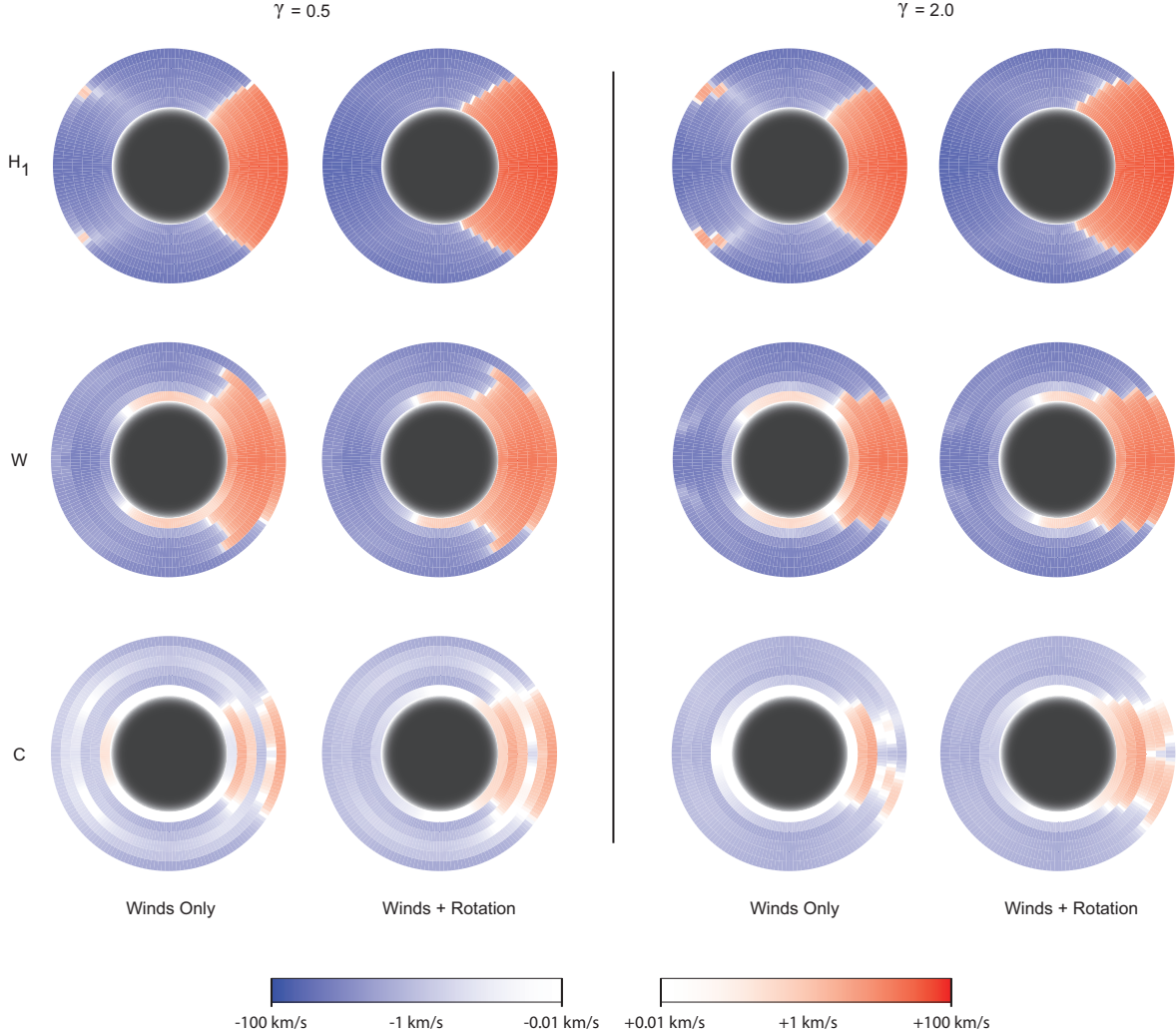


Fig. 4.— Projected average LOS velocities along the observer’s sight line through the atmospheres of models C, W, and H1. Darker blue (red) corresponds to stronger blue (red) shifted winds. For each pair of images, the leftmost includes only the effects of winds, while the rightmost includes the effects of both winds and planetary rotation. The hottest models have the highest wind speeds and the fastest rotation. Max LOS wind speeds for the C, W, and H1 models respectively are 11, 4, and  $0.5 \text{ km s}^{-1}$  ( $18$ ,  $5$ , and  $0.6 \text{ km s}^{-1}$  when rotation is included in the calculation). LOS velocities have been calculated at each of 6 pressure levels – 1 bar, 0.1 bar, 0.01 bar, 1 mbar, 0.1 mbar, and 0.01 mbar. Pressure increases from the outermost annulus, inward to the dark circle at the center of each image, which represents the optically thick interior of the planet. This figure is not to scale.

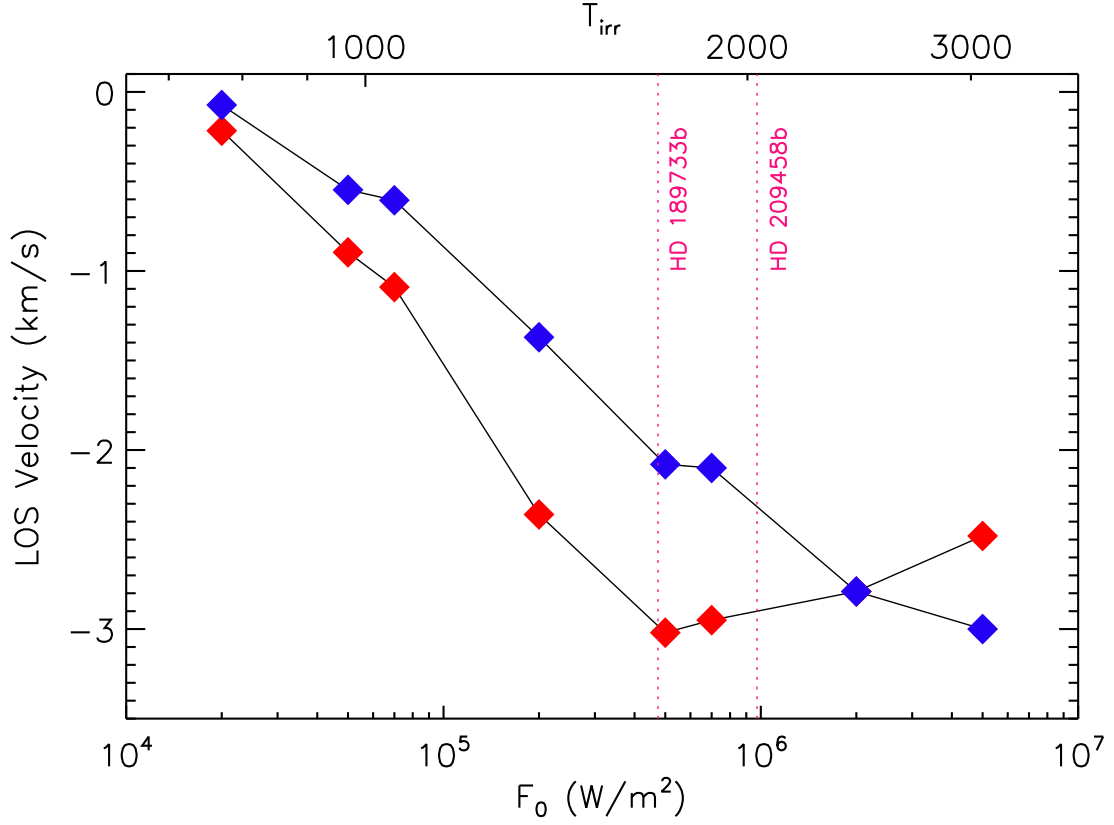


Fig. 5.— LOS velocities for each of the 16 models studied in this paper, obtained by cross-correlating the fully Doppler shifted transmission spectra against an unshifted template spectrum. Models with temperature inversions ( $\gamma = 2.0$ ) are shown in red. Those without T-inversions ( $\gamma = 0.5$ ) are shown in blue. The irradiation levels for the hot Jupiters HD 209458b and HD 189733b are indicated.

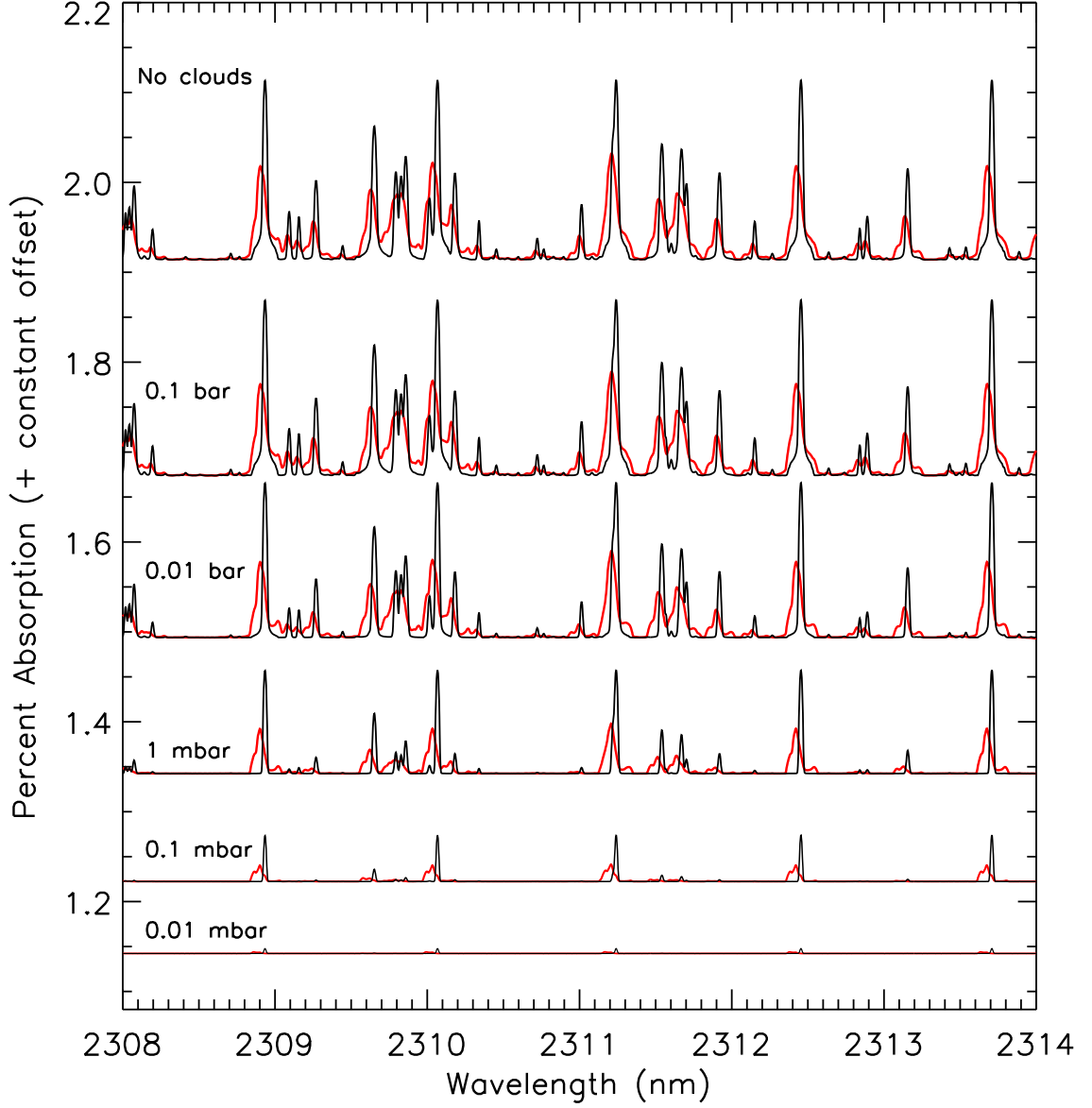


Fig. 6.— Transmission spectra for the second hottest model of our suite (Model H) with  $\gamma = 2.0$ . Optically thick clouds have been inserted at pressures from 0.1 bar to 0.01 mbar. Spectra without Doppler shifts introduced are in black, and those with Doppler shifts caused by clouds and planetary rotation are in red. The reduction in line strength for clouds at higher altitude results from stellar light permeating a much reduced portion of the atmosphere.



Table 1. Relevant parameters for each of the models

Model	$\mathcal{F}_0$ (W m <sup>-2</sup> )	$T_{irrad}$ (K)	$\Omega_p$ (s <sup>-1</sup> )	a (AU)
C	$2 \times 10^4$	771	$1.3 \times 10^{-6}$	0.28
C1	$5 \times 10^4$	969	$2.6 \times 10^{-6}$	0.17
C2	$7 \times 10^4$	1054	$3.4 \times 10^{-6}$	0.15
W	$2 \times 10^5$	1370	$7.5 \times 10^{-6}$	0.09
W1	$5 \times 10^5$	1723	$1.5 \times 10^{-5}$	0.06
W2	$7 \times 10^5$	1874	$1.9 \times 10^{-5}$	0.05
H	$2 \times 10^6$	2437	$4.2 \times 10^{-5}$	0.03
H1	$5 \times 10^6$	3064	$8.4 \times 10^{-5}$	0.02